Journal Pre-proofs

Direct contact ultrasound for fouling control and flux enhancement in Air-Gap Membrane Distillation

Osamah Naji, Raed A. Al-juboori, Les Bowtell, Alla Alpatova, Noreddine Ghaffour

Please cite this article as: O. Naji, R.A. Al-juboori, L. Bowtell, A. Alpatova, N. Ghaffour, Direct contact ultrasound for fouling control and flux enhancement in Air-Gap Membrane Distillation, *Ultrasonics Sonochemistry* (2019), doi: https://doi.org/10.1016/j.ultsonch.2019.104816

This is a PDF file of an article that has undergone enhancements after acceptance, such as the addition of a cover page and metadata, and formatting for readability, but it is not yet the definitive version of record. This version will undergo additional copyediting, typesetting and review before it is published in its final form, but we are providing this version to give early visibility of the article. Please note that, during the production process, errors may be discovered which could affect the content, and all legal disclaimers that apply to the journal pertain.
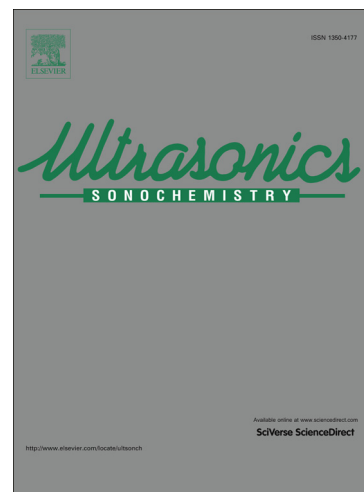
Direct contact ultrasound for fouling control and flux enhancement in Air-Gap Membrane Distillation

Osamah Naji[1,2], Raed A Al-juboori[1,3], Les Bowtell[1], Alla Alpatova[4], Noreddine Ghaffour[4]

[1]*Faculty of Health, Engineering and Sciences, University of Southern Queensland, Toowoomba, Australia, 4350.*

[2]*University of Technology Sydney (UTS), Centre for Technology in Water and Wastewater Treatment, Sydney, NSW, 2007.*

[3]*School of Science, Engineering and Information Technology, Federation University Australia, University Drive, Mt Helen, VIC 3350, Australia* [4]*King Abdullah University of Science and Technology (KAUST), Water.*

[4]*Desalination and Reuse Centre (WDRC), Biological and Environmental Science and Engineering (BESE), 23955-6900 Thuwal, Saudi Arabia.*

Corresponding author: Raed A Al-Juboori, Tel. +61 413424126 Email: RaedAhmed.Mahmood@gmail.com

Abstract

Air Gap Membrane distillation (AGMD) is a thermally driven separation process capable of treating challenging water types, but its low productivity is a major drawback. Membrane fouling is a common problem in many membrane treatment systems, which exacerbates AGMD's low overall productivity. In this study, we investigated the direct application of low-power ultrasound (8-23W), as an in-line cleaning and performance boosting technique for AGMD. Two different highly saline feedwaters, namely natural groundwater (3970 µS/cm) and RO reject stream water (12760 µS/cm) were treated using Polytetrafluoroethylene (PTFE) and polyvinylidene fluoride (PVDF) membranes. Theoretical calculations and experimental investigations are presented, showing that the applied ultrasonic power range only produced acoustic streaming effects that enhanced cleaning and mass transfer. Attenuated Total Reflection Fourier-Transform Infrared Spectroscopy (ATR FT-IR) analysis showed that ultrasound was capable of effectively removing silica and calcium scaling. Ultrasound application on a fouled membrane resulted in a 100% increase in the permeate flux. Cleaning effects accounted for around 30-50% of this increase and the remainder was attributed to mass transfer improvements. Contaminant rejection percentages were consistently high for all treatments (>99%), indicating that ultrasound did not deteriorate the membrane structure. Scanning Electron Microscopy (SEM) analysis of the membrane surface was used to confirm this observation. The images of the membrane surface demonstrated that ultrasound successfully cleaned the previously fouled membrane, with no signs of structural damage. The results of this study highlight the efficient and effective application of direct low power ultrasound for improving AGMD performance.

*Keywords***:** *Membrane distillation, Direct Ultrasound, Fouling control, Cleaning, AGMD, Challenging feedwater and Mass transfer.*

1. Introduction

Membrane distillation (MD) is an emerging desalination process, currently being considered as a viable alternative to conventional desalination technologies such as multi-stage flush and multi-effect evaporation. MD has several economic and environmental advantages, including its ability to operate at low system pressures (<1 bar) and at relatively low feedwater temperatures (< 80°C) [1, 2]. Other economic advantages of the MD process include reduced potential for membrane damage, compared to high pressure-driven processes [3], no

2

requirement for feed water pre-treatment [4] and reduced chemical usage [5]. There are four common designs of MD; direct contact MD (DCMD), air gap MD (AGMD), Sweeping gas membrane distillation (SGMD) and Vacuum membrane distillation (VMD). AGMD is of particular interest to researchers due to its potential for being scaled up to industrial size [6].

Because of their versatility and effectiveness, the use of membrane processes in water treatment and desalination technologies has dramatically increased over the past few decades. However, membrane fouling remains the main issue significantly impeding their overall performance [7]. Depending on the feedwater type, membrane fouling can be classified into four main categories, such as colloidal, inorganic, organic and bio-fouling [8]. As membrane filtration proceeds, fouling materials are accumulated on the membrane surface or within its pores. This negatively affects separation efficiency over extended periods of time [9]. Thus, membrane fouling caused by the accumulation and deposition of salts on the surface of MD membranes due to feed water evaporation can compromise membrane's hydrophobicity and increase pore wetting [10]. The leakage of feedwater through the wetted pores to the permeate side of membrane not only reduces the vapour flux but also promotes salt passage across the membrane significantly deteriorating permeate quality [11, 12].

Historically, a range of different cleaning techniques as well as their combinations have been practiced to control membrane fouling, including mechanical [7], thermal [13], physical [14], and chemical cleaning [15]. The lifetime of a membrane can be significantly reduced due to its contact with aggressive chemicals during chemical cleaning [16]. Additionally, the aggressive chemical cleaning solutions represent a threat to the environment and need to be appropriately treated before their discharge into the environment. Other disadvantages of traditional cleaning methods are reducing surface roughness, changing the hydrophobicity of the membrane, and altering membrane surface charge [17, 18]. With all of these cleaning techniques, the system must also be shut down, and in some cases, the membranes have to be removed, leading to a considerable downtime or costly duplication of filtration systems [19]. Hence, this study proposes the use of *in situ* ultrasonic cleaning technique for AGMD.

Ultrasound is considered as a viable alternative to traditional cleaning methods and has been successfully applied to remove foulants from pressure driven membranes such as reverse osmosis (RO), ultrafiltration (UF) and microfiltration (MF) [20-22]. This cleaning technique is inherently chemically free [23], requires no system shutdown or need for membrane

3

removal from the system for *ex situ* cleaning, which also minimises the membrane's contact with air. Ultrasonic cleaning has minimal effects on the environment and human health and is relatively simple to implement in water treatment systems [24, 25]. It also has the potential of being a beneficial anti-fouling upgrade and efficient at deactivating a wide range of microbes and viruses [26, 27]. Regular *in situ* use of ultrasound can also increase a membrane's operational run-time due to significantly decreased fouling rates [28]. During the ultrasonic process, deposited particles are removed from the membrane surface due to mechanical vibration or by the so-called 'micro-jet' action of collapsing cavitation bubbles [29]. As a result of this cleaning action, the permeate flux through the membrane tends to recover back to pre-fouling levels. However, applying ultrasonic power at a level of cavitation inception can cause damage to the membrane [30]. Ultrasound may also improve the separation efficiency of the membrane as it is known to enhance fluid separation [31-33]. For the case of MD, the separation is governed mainly by mass and heat transfer across the membrane and the vibrational effects of ultrasound can improve both of these phenomena [34].

Despite the fact that some previous studies have explored the use of ultrasound technologies for the alleviation of fouling in MD [35, 36], all of them were conducted with DCMD modules, which is technically an easier task than the application of ultrasound in an AGMD module. Direct contact with the feedwater allows ultrasound to be applied to any 'wet' part of the system and the waves can easily transfer to the membrane through conduction. Additionally, previous investigations explored ultrasound application through a conveying media (the module body or water bath) [35-37]. Such applications can be extremely energy inefficient, as a large part of ultrasonic energy gets absorbed by the conveying media. The case is quite different with an air-gap design, as applying ultrasound through the housing of the membrane does not result in effective propagation of the waves to the membrane. The air-gap is a poor transport path for the ultrasonic energy to be transferred to the membrane, due to the comparatively low viscosity of air. Hence, this study will address the challenge of externally applied ultrasound and demonstrate that although more difficult, the correct direct external application to the membrane surface requires only a small fraction of the power used to achieve the same anti-fouling and permeate flux production enhancements with DCMD. In this study, the ultrasonic transducer is mechanically coupled to the membrane spacers on either side of the membrane cassette.

Our previous research showed a successful application of low intensity magnetostrictive ultrasound with square wave excitation for water treatment [38]. Based on these results, we

now investigate the applicability of the same ultrasound topology at power range of 8 - 23W corresponding to an application intensity of approximately 24 - 68 W/m², for in-line anti-fouling and performance enhancement of an AGMD system for two types of MD membranes; polytetrafluoroethylene (PTFE) and polyvinylidene fluoride (PVDF). The effect of feedwater flow rate and temperature on permeate flux and membrane rejection during the AGMD process is evaluated with respect to two types of feedwater, RO reject water and natural groundwater. Theoretical investigations identifying ultrasound mechanisms for improving membrane performance are also presented. However, developing a detailed mathematical model for simulating ultrasonic-assisted AGMD operation under different treatment scenarios is recommended for future work.

2. Materials and methods

2.1. Sample preparation

RO reject water and natural groundwater samples, henceforth denoted as RW and NW were collected from Dalby Sewage Water Treatment Plant (Dalby, Qld 4405 Australia) and were used as feedwater for the MD system. The physico-chemical characteristics of these water samples are provided by the treatment plant as shown in Table 1.

Table. 1. Properties of feedwater samples.

Characteristics (mg/L)	RW	NW
Ammonia-Nitrogen	<0.005	<0.005
CaCO₃	1,410	-
Chloride	2,900	900
Calcium	190	55
Magnesium	230	70
Sodium	2,070	550
Potassium	5.2	5.1
Nitrate	1.8	0.59
Nitrite	0,005	<0.005
Manganese (dissolved)	<0.001	-
Fluoride	0.51	0.09
Total Nitrogen	0.58	0.67
Total organic carbon	<1.0	<1
Iron (dissolved)	<0.01	-

Barium	0.053	0.056
Solids (total)	1900	1900
SiO3	180	160
Sulphate	140	150
Total Sodium	730	550
Total Alkalinity (meq/L)	-	324
Bicarbonate Alkalinity (meq/L)	-	324
Conductivity (µS/cm)	12,760	3,970
Total Dissolved Solids	-	1900

2.2. Membrane specifications

PTFE laminated on typar 3161L and PVDF membranes without a support layer were used in the experimental work. These two membranes are commonly used in MD processes due to their hydrophobicity, thermal stability and mechanical durability to withstand ultrasound vibration [35, 39, 40]. Both membranes were supplied by Donaldson Filtration Solutions. The main characteristics of the membranes are shown in Table 2. The dimensions of the membrane cassette were as follows: 42 cm (length) × 1 cm (thickness) × 24 cm (width). Membranes were installed on both sides of the cassette with the total effective surface area of 0.2016 m^2.

Table 2: Characteristics of the PTFE and PVDF membranes

Specification	PTFE membrane	PVDF membrane
Material	PTFE	PVDF
Support	Laminated on typar 3161L spunbond polypropylene	None
Pore size (µm)	0.3	0.3
Thickness (µm)	254	154
Porosity (%)	75	80
Contact angle (º)	114	97.4

2.3. Experimental setup

The AGMD setup used in this investigation is demonstrated in Fig. 1. As illustrated in Fig.1 a, the setup is consisted of two thermally insulated tanks with a capacity of 33 L each for carrying feedwater and coolant water. The water flow from the feed and coolant sides into the membrane module via their respective 12 mm automotive grade rubber hoses. The hoses

6

were lagged with the pipe insulation to reduce heat losses. Two rotameters (variable area flow meter type 335, 4 - 20 mA output, 0 - 500 L/hr, supplied by George Fischer) were utilized to measure the feedwater and coolant water flow rates. Two centrifugal immersion pumps (Precision Immersion Heater Circulator, 24Volt dc, supplied by Ratek) were used to circulate the heated feedwater and the coolant water in a batch mode.

The AGMD module was machined from aluminium and was equipped with 316 grade stainless steel fittings. Seven industrial-style temperature probes (RTD sensor - Pt100 type with pot seal, supplied by TC Direct) were installed onto different locations along the water flow pathways; four on the feedwater side and three on the coolant side to monitor temperature in the AGMD system. The temperature controller accuracy was ± 2°C. Pressure sensors (Wika type DP250, 0 - 250 mbar, 4 - 20 mA output, supplied by Wika) were connected through isolation transmitters to the feed inlet and outlet of the AGMD module in order to monitor the pressure in AGMD system. Two conductivity sensors (Microchem Conductivity Transmitter, supplied by TPS +/- 4.0μS/cm) were used to measure the conductivity in the feed and coolant tanks to determine the rejection percentage. An electronic balance with serial interface (model PA64C, supplied by Technical Advantages) was used to record the mass of produced permeate. All sensors were connected to an industrial PLC/SCADA system for control data logging and display purposes.

The feed and coolant compartments of the AGMD module were connected to the respective heating and cooling systems. The membrane cassette was precisely located between the two compartments with the selective layer of the membrane facing the feed side of module. An air gap of 2 mm between the other side of membrane and coolant side was maintained using 1 mm thick in-house made 316 stainless steel metallic spacers on both sides (Fig1 b). The spacers dimensions are similar to those of the membrane with a thickness of 1 mm. The feed solution flows between the membranes placed on either side of the cassette module and permeate was ultimately collected in the permeate tank via the cassette module outlet pipe located at the lower end of the module.

Fig.1 c shows two ultrasound transducers (model CU18A, Etrema Products, Inc.) were mounted externally on the AGMD module resting on rubber discs. The ultrasonic transducers were connected to the spacers through two metallic screws. Ultrasonic power was controlled using a system shown in Fig.1 (c). Detailed description of the system can be found elsewhere

7

[38]. The ultrasonic power applied in this study ranged between 8 W (intensity $\approx$ 24 W/m^2) and 23 W (intensity $\approx$ 68 W/m^2) in a continuous mode at a fixed frequency of 17.8 kHz (resonance frequency). Continuous mode is likely to be more effective than the pulsed mode in ultrasonic-assisted AGMD applications. Pulsed mode is normally applied as an energy saving mode for high power ultrasonic applications where cavitation occurs [41]. Pulsed mode ultrasound improves cavitational effects by enlarging the effective zone of cavitation and reducing shielding effects [42, 43]. The occurrence of cavitation is unexpected with the low power level applied in this study, thus continuous mode was selected for conducting the experimental work. Although testing various frequency levels is not covered in this investigation, it is worth mentioning that increasing ultrasonic frequency may deteriorate the structural properties of the membrane, especially for frequencies greater than 20 kHz [44]. It was found that increasing the frequency from 20 kHz to 68 kHz negatively affected the permeate flux of DCMD [35]. Also, in order to compare system efficiency fairly at different treatment frequencies, the transducers and spacer plates used to transfer the ultrasonic energy, need to be at resonant frequency, requiring a design and equipment change for each frequency applied. Hence, a single low frequency level was applied in this initial investigation, not discounting the possibility of further work in this area.
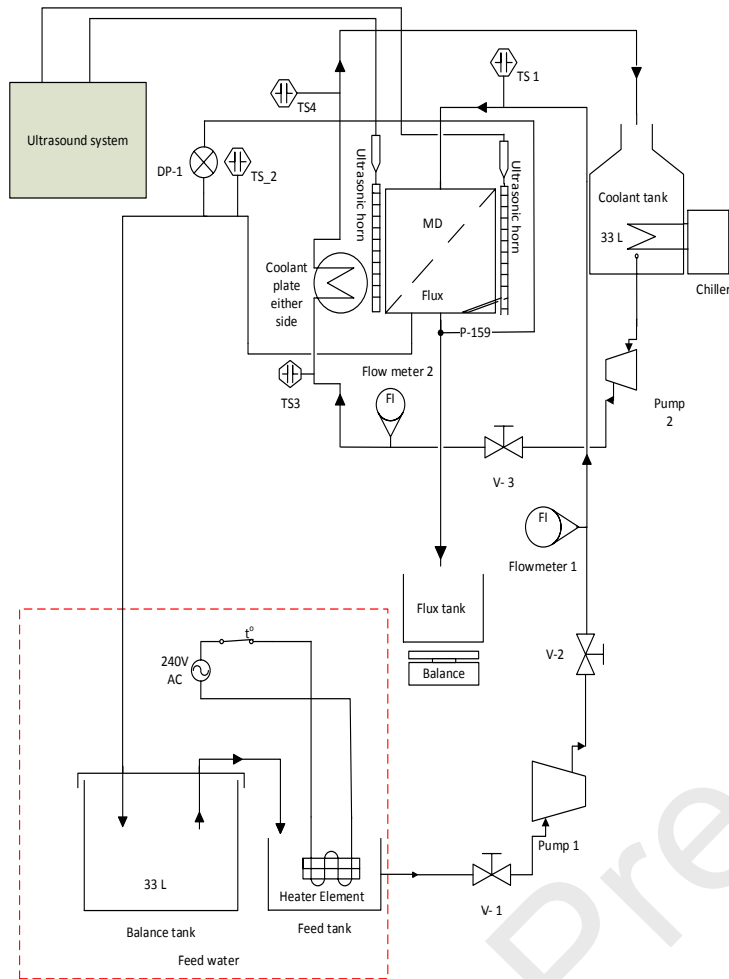
Item	Description
Pump 1	submersible Model: LVMI3I 24 Volt DC-2.5 Amp flow rate 4 L/min
Pump 2	submersible Model: LVMI3I 24 Volt DC-2.5 Amp flow rate 4 L/min
V1	manual valve, control on the flow rate on/off heat side
V2	Manual valve, control on the flow rate, heat side
V3	Manual valve, control on the flow rate, coolant side
Flow meter 1,2	Variable area flow meter type 335 range 50-500 L/hr
TS	RTD Sensor -Pt100 with Pot Seal, Operating range: -75ºC to +350ºC, 3mm dia x 100mm long
DP-1	Wika, Differential pressure transmitter, Model: DP-10 Range: 0-250 mbar
Chiller	Model: RC1, Volt: 240 V/50Hz,Range: 0-30ºC
Heater	Range 0-90ºC
Ec-1	0 to 1 V DC or 0 to 5 V DC Outputs, k=1.0 Sensor....0 to 19.99 uS/cm
Ec-2	0 to 1 V DC or 0 to 5 V DC Outputs, k=0.1 Sensor....0 to 19.99 uS/cm
Ion Fl	0.02 to 19,000 mg/L F-, -0 to 60 ºC (32 to 140 ºF

(a)

(b)

<table>
<tr><td>(c)</td><td>(d)</td></tr>
</table>

Fig. 1: AGMD setup: (a) Schematic representation (b) metallic spacer, (c) AGMD module connected to ultrasonic transducers and (d) ultrasound control system.

2.4. Experimental procedure

The AGMD process with no ultrasound cleaning was run for 70 h with feed temperature of 70°C, feedwater flow rate of 100 L/h, coolant temperature of 20°C and coolant flow rate of 200 L/h. The permeate flux was measured every 10 h. After 70 h of operation when the permeate flux decreased by around 50% on both membranes (Fig. 3), ultrasound was then applied for 15 minutes. It should be mentioned here that an ultrasonic power range of 8-23 W was applied for studying the effect of varying power level on permeate flux production. The power was measured using a wattmeter (EDMI MK7C Single Phase Smart Meter) and an oscilloscope (Tektronix, TPS2014) supplied with current probe (Tektronix, TCP 202), control was achieved with the arbitrary function generator (Tektronix AFG 30 2208) producing the waveform signal for the audio power amplifier (Peavey IP 8.5-C). The effect of feedwater temperature and flowrate on permeate flux and rejection were tested. Three different feed temperatures of 50°C, 60°C and 70°C were applied along with three different flow rates of 50 L/h, 100 L/h and 150 L/h. The coolant flow rate and temperature were fixed at 200 L/h and 20°C, respectively. Experiments were conducted in triplicate to ensure the repeatability of the work.

2.5. Analytical methods

The respective conductivities of the feed and permeate samples were measured by Microchem Conductivity sensor/transmitters (supplied by TPS Pty Ltd), the millivolt signals were transmitted into the PLC analogue card to allow logging with the SCADA system. A scanning electron microscopy (SEM Model JCM-6000 BENCHTOP, supplied by JEOL) was used to examine the membrane for potential changes in morphology structure as a result of

membrane fouling and/or exposure to ultrasound treatments. A Fourier transform infrared (FT-IR) spectrometer (Model IR Affinity-1S, supplied by SHIMADZU) with an attenuated total reflectance (ATR) accessory was used to study the surface chemistry of virgin, fouled and cleaned membranes.

3. Fouling mitigation and flux enhancement-ultrasound mechanisms

The extent of ultrasonic effect on AGMD process in the present configuration (Fig.1) depends on the applied ultrasonic parameters and the medium being irradiated. In the case of AGMD, there are three media; water, membrane and a mixture of air and vapour. The effect of ultrasound in the latter two is in the form of acoustic streaming. However, chemical, extreme localised physical effects (i.e. high temperature and pressure) and mechanical effects such as micro jets and shock waves may occur in water due to the generation and subsequent collapse of cavitating bubbles [45]. Cavitational bubbles can only occur when the applied ultrasonic pressure for given conditions of irradiated liquid exceeds the cohesive forces of the liquid. This can be determined through calculating cavitation threshold using equations 1 and 2 [28, 46]:

$$P_b = P_o + \frac{2}{3}\sqrt{\frac{\left(2\sigma/R_o\right)^3}{3\left(P_o + 2\sigma/R_o\right)}} \tag{1}$$

$$P_A = \sqrt{2I\rho C} \tag{2}$$

where P_b is the cavitation threshold pressure (Blake threshold) (Pa), P_o is the pressure of the water without ultrasound effect (Pa), σ is the water surface tension (N/m), R_o is the initial bubble radius (m), P_A is the acoustic pressure (Pa), I is the ultrasonic intensity (W/m^2), ρ is the water density (kg/m^3) and C is the sound velocity in the irradiated medium.

Given the low ultrasonic power applied in this study, the occurrence of cavitation is unlikely, and this will be discussed further in section 4. In this case, the ultrasonic effect across all the media involved in mass transfer is non-cavitational, or in other words, acoustic streaming. The acoustic streaming can prevent foulants deposition on membrane by counteracting the adhesion forces such as drag force and electrostatic interactions. It can also alter the nature of

11

the flow across the membrane to become turbulent and this in turn reduces temperature and concentration polarization and consequently improve mass transfer across the membrane [6]. Theoretical representation for the effect of ultrasound on mass transfer is provided in the following part of this section.

Acoustic streaming can influence the resistance across the membrane as illustrated in Fig. 2. An analogy to electrical resistors is usually made to depict the resistance components in membrane distillation process [6, 47]. The resistance of the flow is the inverse of mass transfer coefficient. The overall mass transfer across AGMD can be expressed by the following formula [6];

$$J = K(P_{fm} - P_{sm}) \tag{3}$$

Where J is the permeate flux (kg/m^2.s), K is the overall membrane transfer coefficient and it is the combination of mass transfer coefficient of feed (K_f), membrane (K_m) and strip side (K_s) (J/Pa) and P_{fm} and P_{sm} are respective vapour pressures at membrane interface for feed and strip sides.
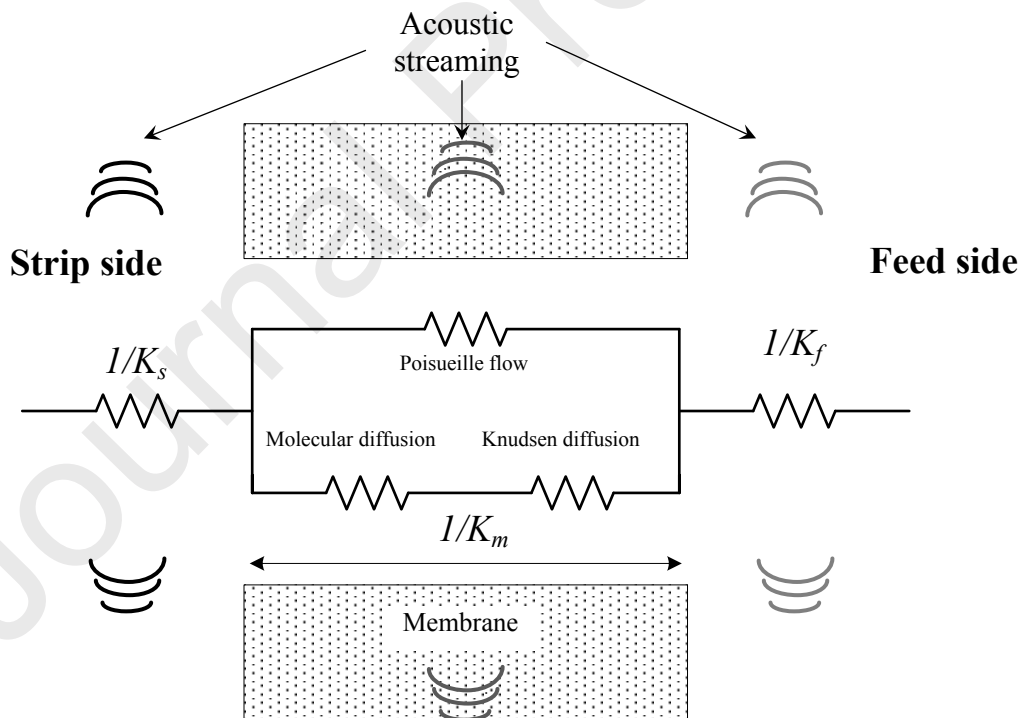

Fig. 2: Ultrasound effect on mass transfer across AGMD module

As demonstrated in Fig. 2, acoustic streaming can travel to the strip side and across the membrane to the feed side, but might lose some of its energy through the membrane and

feedwater represented by the fading colour of the waves. The lost ultrasonic energy is absorbed by the transverse media, which can be quantified applying an exponential power law (equation 4) [48].

$$\ln\left[\frac{I}{I_\circ}\right] = -\alpha d \tag{4}$$

Where I_0 and I are initial and attenuated ultrasonic intensity (W/m^2) for a travelling distance of d (m) and α is attenuation coefficient of the absorbing media (dB/m).

The feed side mass transfer coefficient can be calculated applying Sherwood number (*Sh*) formula given by 5 [49];

$$Sh = \frac{K_f d_h}{D} \tag{5}$$

D is the molecular diffusivity (m^2/s) and d_h is hydraulic diameter (m).

Based on the flow conditions, Sherwood number can be computed applying empirical relations given in 6 and 7 [50];

$$Sh = 0.13\, Re^{0.64}\, Sc^{0.38} \qquad Re{<}2100 \tag{6}$$

$$Sh = 0.023\, Re^{0.8}\, Sc^{0.33} \qquad Re{>}2100 \tag{7}$$

Reynolds number represents the proportion of the inertial force to the resistive force. For the case of normal AGMD process, the inertial force is expressed by the flow of the fluid [51]. As stated earlier that acoustic streaming acts as inertial force that introduces turbulences into the flow as enunciated in equation 8 [52, 53];

$$Re_{US} = \frac{\rho a \omega d_h}{\mu} \tag{8}$$

where a is the ultrasonic displacement amplitude (m), *??* is the angular frequency (Hz), ρ is fluid density (kg/m^3) and μ is the fluid viscosity (Pa.s) and subscript *US* denotes flow conditions under ultrasound effects.

Mass transfer through the membrane in AGMD configuration can be explained by three mechanisms; Poiseuille flow, molecular diffusion and Knudsen diffusion [6, 54]. However, only the latter two occur in AGMD. The prominent transfer mechanism can be identified

through computing Knudsen number (K_n) (9) [51]. If K_n <0.01, the molecular diffusion dominates. If 0.01 <K_n < 10, the diffusion of the vapour falls in the molecular-Knudsen diffusion region. For flow with K_n >10, Knudsen diffusion mechanism is prevalent [6, 55].

$$k_n = \frac{K_B T_{av}}{\pi d_p [0.5\,(\sigma_w + \sigma_a)]^2 P_t} \cdot \frac{1}{\left[1 + \frac{M_w}{M_a}\right]^{0.5}} \tag{9}$$

where d_p is the pore diameter(m), K_B is Boltzmann constant, 1.380 ×10^{-23} (J /K), σ_w and σ_a the collision diameters of water (2.7 × 10^{-10} m) and air (3.7 × 10^{-10} m), respectively, P_t the total gas pressure in the membrane pores (Pa), and M_a is the molecular weight of air (~ 29 kg/ kmol) and M_w is the molecular weight for water (18 kg/kmol).

Mass transfer coefficient for molecular diffusion, Knudsen diffusion and molecular-knudsen diffusion can be expressed by 10,11 and 12, respectively [6, 56, 57];

$$k_m = \frac{P_{av}}{P_{a(lm)}} \cdot \frac{\varepsilon}{\delta\chi} \cdot \frac{D_w M_w}{RT} \tag{10}$$

$$k_m = \frac{M_w}{RT} \cdot \frac{2\varepsilon r}{3\delta\chi} \cdot \left[\frac{8RT}{\pi M_w}\right]^{0.5} \tag{11}$$

$$K_m = \frac{M_w}{RT} \cdot \frac{\varepsilon PD}{\delta\chi} \ln\left[\frac{P_{a1}\frac{2r}{3}\left[\frac{8RT}{\pi M_w}\right]^{0.5} + PD}{P_{a2}\frac{2r}{3}\left[\frac{8RT}{\pi M_w}\right]^{0.5} + PD}\right] \tag{12}$$

where R is universal gas constant, 8.314 J/mol.K, P (Pa) and T (K) are the respective average pressure and temperature in the pore, ε the membrane porosity, r is pore radius (m), δ the membrane thickness (m) and χ is membrane tortuosity, $P_{a(lm)}$ is the log-mean air pressure in the pores (Pa) and P_{a1} and P_{a2} are the partial pressures of air at the two sides of the membrane.

Mass transfer coefficient of the strip side can be determined applying equation 13 [58].

$$K_c = \frac{P}{P_{a(lm)}} \cdot \frac{\varepsilon}{\delta\chi + b} \cdot \frac{DM_w}{RT} \tag{13}$$

where b is the air gap thickness (m).

14

It can be noticed that mass transfer coefficients across the membrane and the strip side rely on the intrinsic properties of the medium, pressure and temperature. Acoustic streaming can reduce temperature polarization [59], and this in turn affects medium properties.

4. Results and discussion

4.1. AGMD performance with virgin membranes

The changes in vapor flux as a function of the AGMD process time on PVDF and PTFE membranes with respect to two different types of feedwater; NW and RW are shown in Fig. 3. It should be noted here that all the presented data in the results section are in mean values of three data pointes. PVDF membrane exhibited better performance as compared to PTFE membrane for both water types. Previous studies reported that PTFE has a higher flux compared to PVDF due to its higher mass transfer coefficient [39, 40], however, the observed trend in this study could be attributed to the presence of support layer in the PTFE structure which is absent in PVDF and slightly higher porosity of the latter compared to PTFE. The support layer might add additional hydraulic resistance to the permeate flow. Higher permeate fluxes were observed in AGMD process with NW as opposed to RW regardless of the membrane type. This could be ascribed to a lesser fouling potential of the NW compared to RW. As shown in Table 1, RW has more than three times inorganic contamination load as that of NW expressed by conductivity measurements (12,760 µS/cm vs 3,970 µS/cm). The permeate flux of RW for both membranes was lower by 13% compared to NW. A similar trend was observed by Alklaibi and Lior [60] when the feed water concentration increased from 3,120 µS/cm to 78,000 µS/cm.
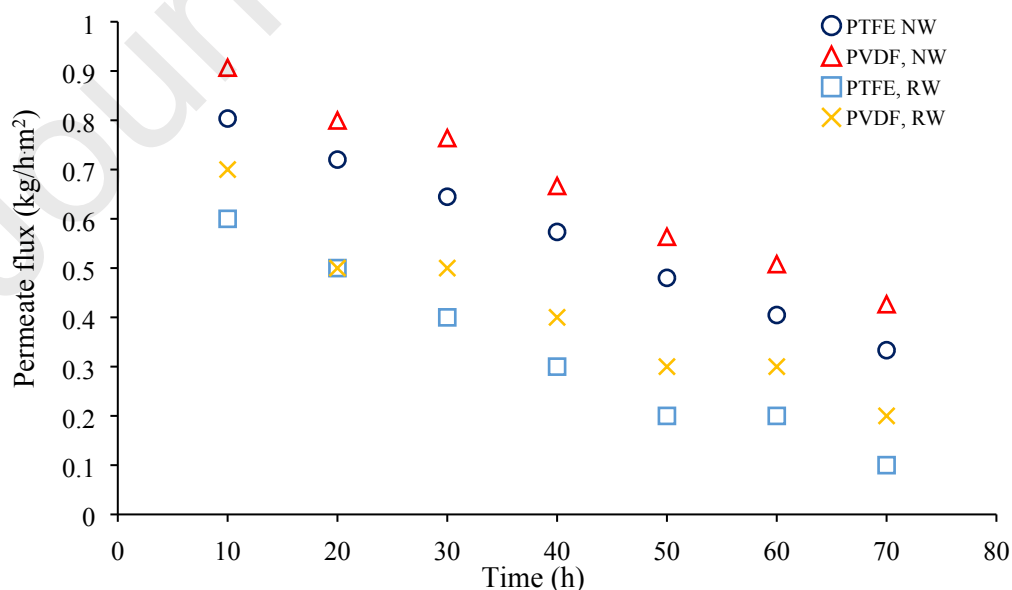
Fig. 3. Permeate flux versus time, PTFE and PVDF membranes type NW and RW.
Feed temperature = 70°C at 100 L/h, Coolant = 20°C at 200 L/h.

4.2. Effect of feed temperature on permeate flux

Figures 4 and 5 present the permeate flux as a function of the feed temperature in AGMD process with, without (silent conditions) and after ultrasound application for the PTFE and PVDF membranes tested for treating NW and RW, respectively. As illustrated in Fig. 4 a in arrows that the primary y-axis represents flux data, while the secondary y-axis illustrates rejection (%) data of cleaned membranes. The cleaning effect of ultrasound is depicted as the difference between the flux curves of before and after US application, while the difference between the flux curves of during and after US application represents mass transfer improvement induced by US. These illustrations apply to Figures 4 - 7, however they are not presented on all figures to avoid unnecessary repetition.

As shown in Fig. 4, permeate flux increased with increasing feedwater temperature from 50 °C to 70°C for both membrane types. This attributed to the nature of MD process as the driving force is the temperature gradient across the membrane, which generates vapour pressure difference across the membrane [61]. As such, the increase in feedwater temperature enhances the driving force of the AGMD process and improves permeate flux production. However, the extent of the permeate flux increase is affected by the overall feedwater temperature. Thus, the increase in permeate flux observed when the feedwater temperature was increased from 50°C to 60°C, was smaller compared to the temperature increment from 60°C to 70°C. As is commonly known, water vapour pressure increases exponentially with temperature [61]. Accordingly, the increment of water vapour pressure would be greater when the temperature was raised from 60°C to 70°C compared to 50°C to 60°C. Increased feedwater temperatures tend to reduce temperature polarization [47, 62]. Therefore, increasing feedwater temperature to 70°C would not only reduce the heat losses associated with the temperature polarization, compared to those at lower feedwater temperatures, but also show improvements corresponding to permeate fluxes and process efficiencies.

When comparing permeate fluxes achieved for NW and RW, it can be seen that permeate flux for NW was higher than that obtained with RW. Since the conductivity of the NW was significantly lower than that of the RW indicating low contaminants concentration, according

to Raoult's law (equation 14 [6]), its vapour pressure would inherently be higher at any tested feedwater temperature than that of the RW. This leads to high vapour productivity of NW compared to RW.

$$P_f = x_w P_w^°$$ (14)

Where P_f is the vapour pressure of the feedwater (Pa), x_w is water molar fraction and $P_w^°$ is the vapour pressure of pure water (Pa).

The application of the ultrasound treatment to enhance the AGMD process resulted in significant increases in permeate flux for both PTFE and PVDF membranes for both water types tested.

It can be noticed that the cleaning effect of ultrasound was almost independent of the feedwater temperature for all treatment scenarios. Similar trend can be seen for mass transfer enhancement of RW, however, the case is different for NW as enhancement increased with increasing the feed temperature. This can be explained by the high concentration of salts in RW that affect the vapour pressure development and consequently the flux (equation 14).

When ultrasound applied after 70 hours of AGMD operation, the fouled membrane's permeate flux recorded was noticeably higher than any of those obtained without ultrasound treatment. Ultrasound cleaning of the two tested membranes resulted in a maximum increase of 50% in NW and RW for the first two temperatures and a little less for the highest temperature. The combined mass transfer improvement and membrane cleaning resulted in doubling the flux for all membranes and water types. Superior performance of the AGMD process was also achieved when ultrasound treatment was applied continuously. These results are in agreement with previous investigation by [37] where permeate flux of MD was reported to reach up to 200 % when an ultrasonic intensity in a range of 0 - 50 kW/m^2 (0 - 5W/cm^2) was applied. However, the intensity applied in this study was much lower, as reported in [37]. The high performance of ultrasound in this study is attributed to the direct application of ultrasound through the spacers where losses are minimal. The attenuation across membrane, feedwater and air and vapour zones, were calculated using equation 4. It

17

was found that the collective attenuation of ultrasonic power across the aforementioned media was very low, in the range of milliwatts, for the highest intensity applied.

The results presented here showed that ultrasound application is not only capable of removing the fouling layer formed on the membrane surface [63], but also aids in preventing foulants from further being deposited and at the same time enhancing the mass transfer across the membrane [30], discussed further in section 4.4. It is noteworthy that the application of ultrasound irradiation does not directly affect the intrinsic membranes permeability [7, 64]. However, it is expected to promote permeate flux by alleviating concentration and temperature polarisation, thereby decreasing membrane fouling and improving mass transfer across the membrane [65]. The improvement of the flux with the aid of ultrasound was also reported in [30, 66]. It should be mentioned here that although applying high power ultrasound improves flux significantly, it negatively affects the membrane structural integrity and leads to damage or pore dilation [30, 35]. Therefore, this study advises against the use of high-power ultrasound as the power effect on mass transfer is not of a linear nature (further details are provided in section 4.4.). The effect of the applied ultrasonic power on membrane integrity was gauged by measuring the reject percentage which showed no difference after ultrasound applications as shown in Figs. 4-7. Further evidence of maintaining membrane integrity will be provided in later sections.
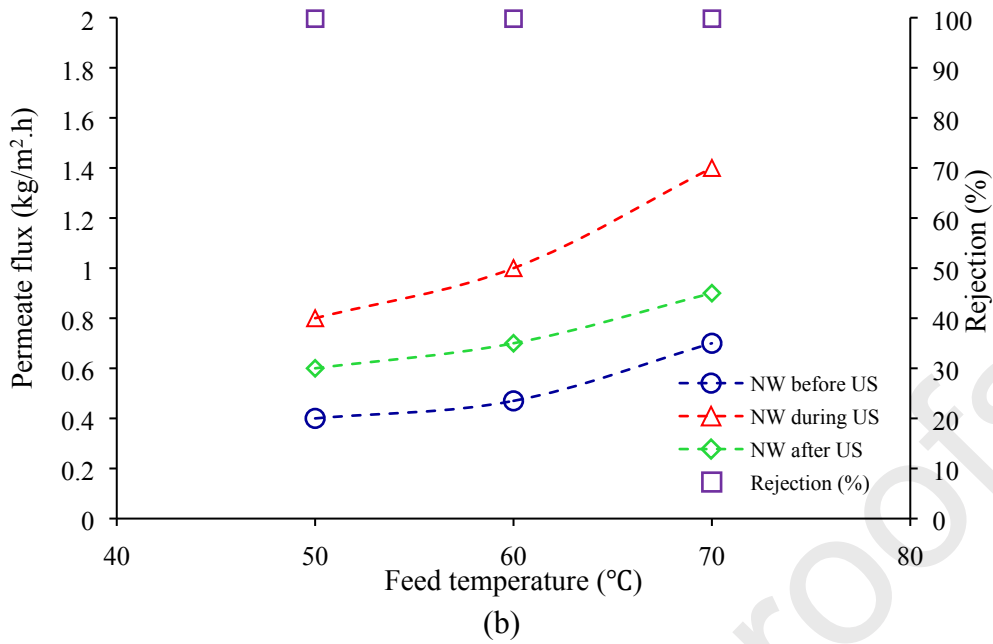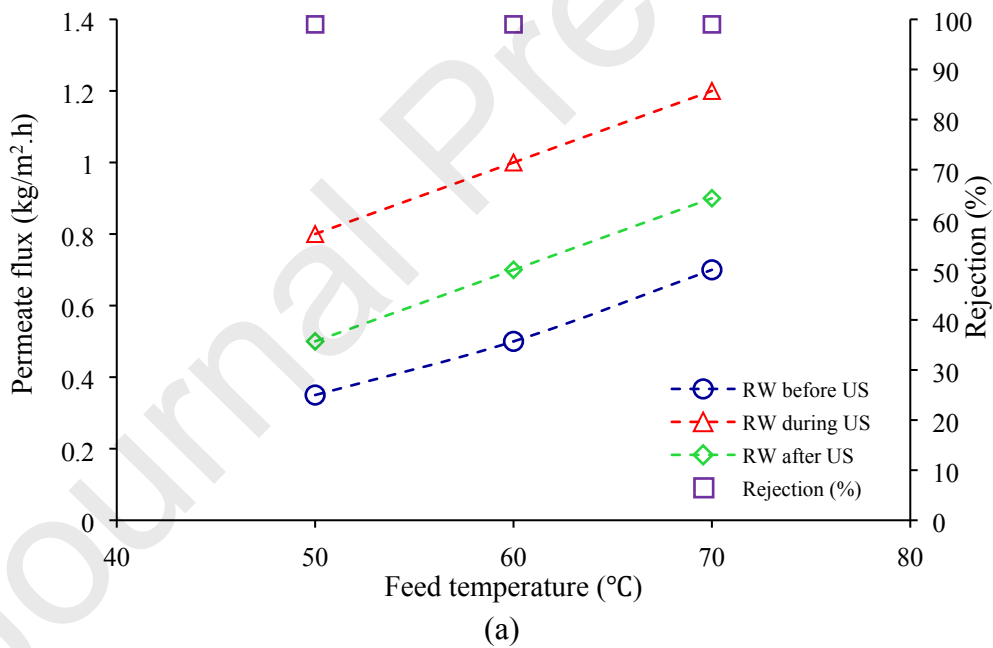

(a)

(b)
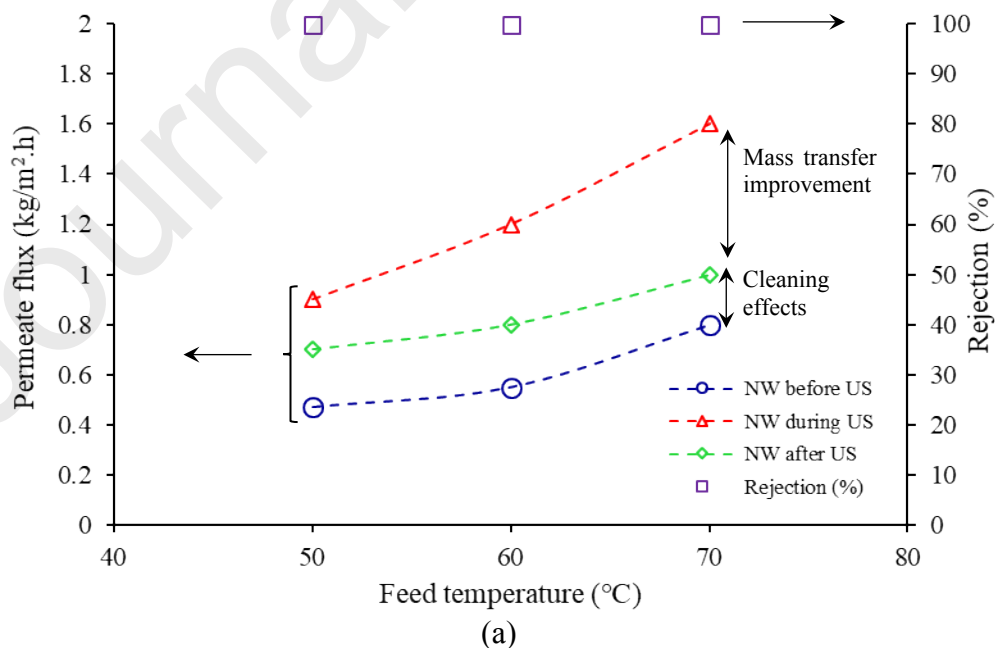
Fig. 4. Ultrasound effect vs permeate flux, NW with different temperatures (a) PVDF, (b) PTFE. Feedwater = 150 L/h, Coolant = 20°C at 200 L/h, ultrasound = 24 W/m^2.
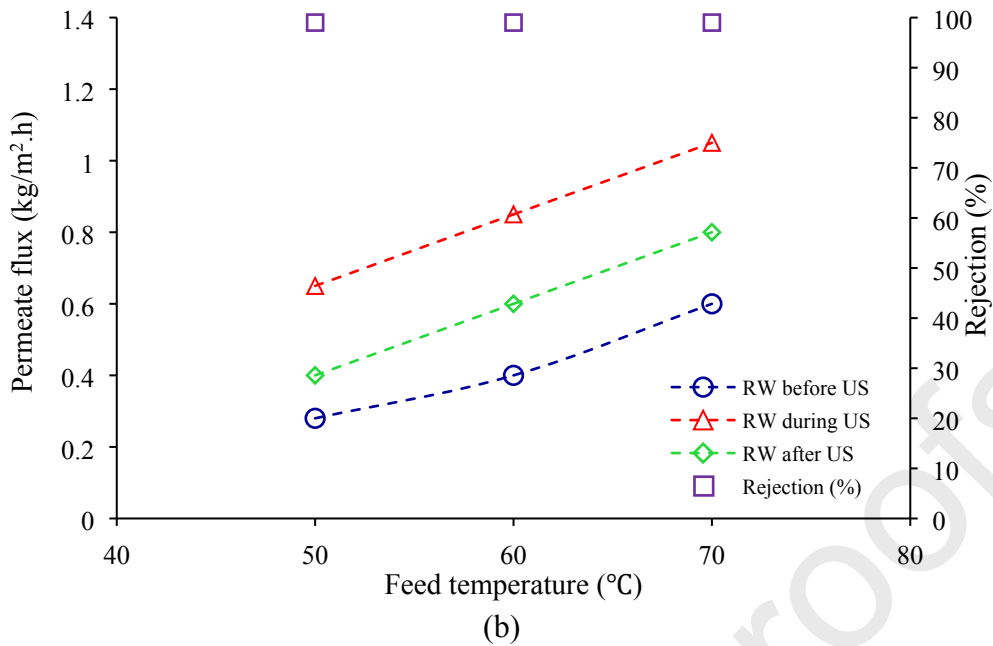

(a)

19

(b)

Fig. 5. Ultrasound effect vs permeate flux, RW at different feed temperatures, (a) PVDF and (b) PTFE. Feedwater = 150 L/h, Coolant = 20°C at 200 L/h, ultrasound = 24 W/m².

4.3. Effect of feed flow rate on permeate flux

The feedwater flow rate is an important parameter which significantly influences the efficiency of the MD process [67]. The feedwater flow rate affects temperature and concentration polarization at the membrane surface [60, 68]. The effect of feedwater flow rate in a range of 50 -150 L/h on the permeate flux with, without and post ultrasound treatment was investigated for PTFE and PVDF membranes using NW and RW samples and the results are shown in Fig.6 and Fig.7, respectively. The permeate flux of the AGMD process increased with feedwater flow rate and ultrasound power for all tested conditions. However, the rate of increase was higher when the feed flow rate was increased from 100 L/min to 150 L/min, compared to that of 50 L/min to 100 L/min. The observed effect can be explained as follows; the feedwater residence time in the AGMD module at low flow rates is longer than that at high rates, leading to a decrease in the temperature gradient across the module, due to the increase in boundary layer thickness, corresponding to temperature and concentration polarization [60].

It can be observed that ultrasound cleaning resulted in an almost 50% increase in the flux for all treatments. The increment rate of NW flux due to ultrasound cleaning was largely the same for all tested flow rates. However, the improvement of RW flux was more pronounced for high flow rates than for low flow rates. This can be attributed to the high salinity of RW,

20

where a high flow rate, combined with acoustic streaming effects, generate higher turbulence that reduces concentration polarisation at the membrane surface and results in less adherence of foulants [69]. Mass transfer improvements resulted in further increases of the flux up to 100% above control. The flux rate increase became sharper when the flowrate increased from 100 to 150 L/h, and this again confirms the impact of the synergistic effect of flow generated and ultrasound induced turbulences, that help in improving vapour transfer across the membrane. The rejection rate was consistently higher than 99% for all treatments.
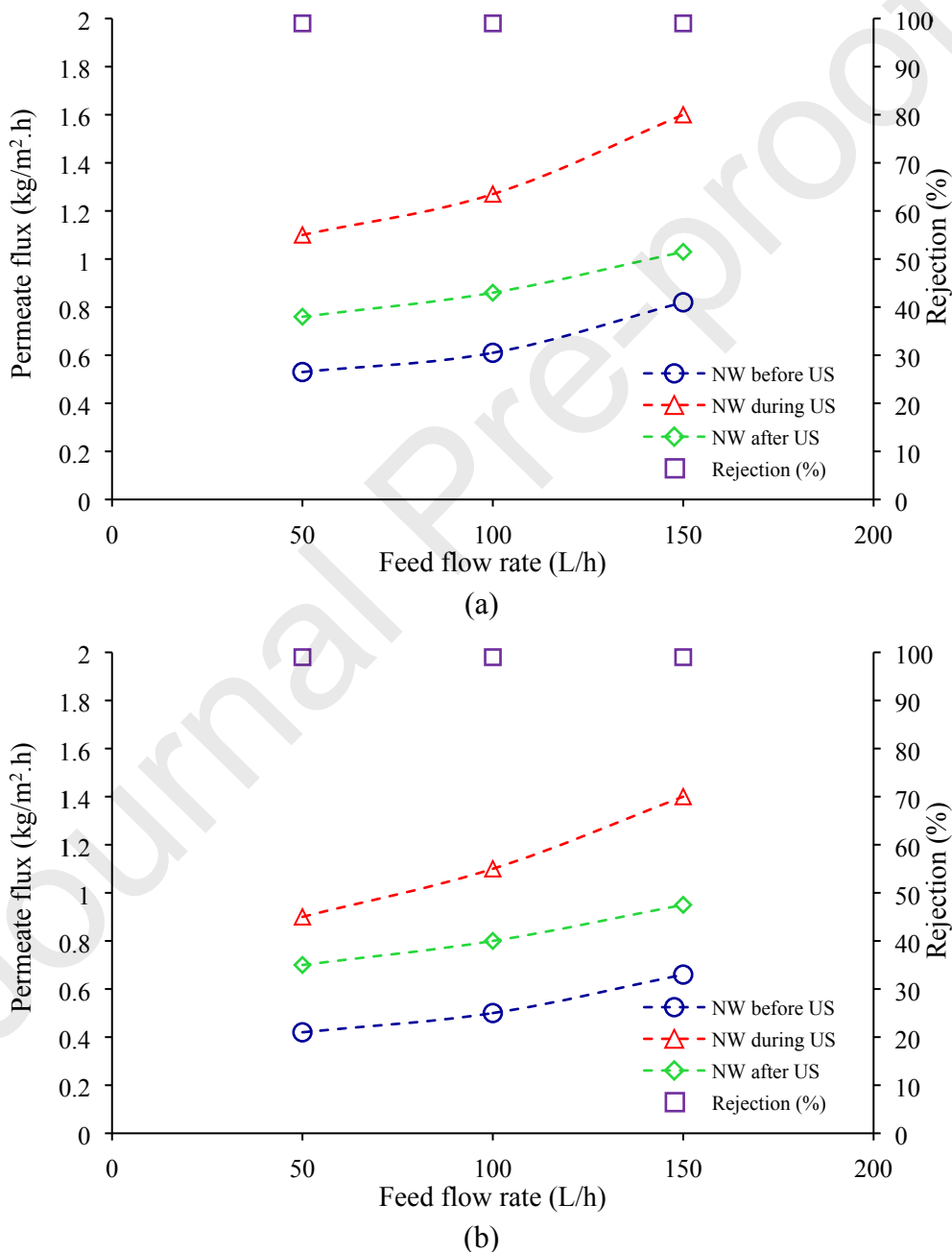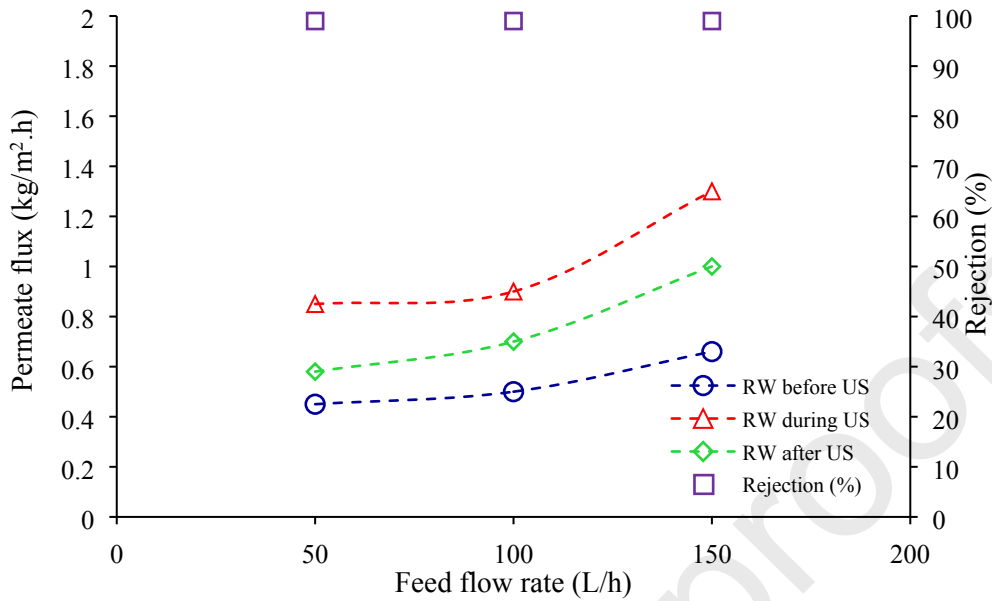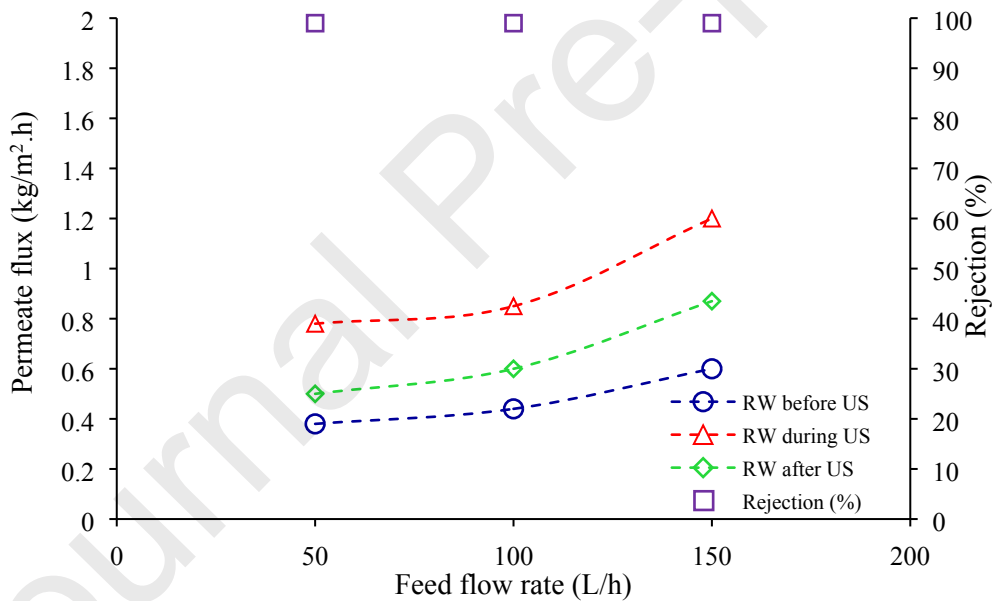

(a)

(b)

Fig. 6. Ultrasound effect on permeate flux: NW with different Feed flow rates (a) PVDF

(b) PTFE. Feed water = 70°C, Coolant = 20°C at 200 L/h, ultrasound power = 24 W/m².

(a)

(b)

Fig. 7. Ultrasound effect on permeate flux, RW with different feedwater flow rates (a) PVDF, (b) PTFE. Feed water = 70°C, Coolant = 20°C at 200 L/h, ultrasound = 24 W/m².

4.4. Ultrasound power effect on permeate flux

Prior to analysing the effect of power increase on AGMD flux, it is important to study ultrasonic effects that are likely to occur within the applied experimental conditions. As stated in section 3, Blake threshold pressure was calculated for the highest power level applying equation 1 and 2 and compared to that of the acoustic pressure generated by

ultrasound as demonstrated in Fig. 8. The initial bubble diameter was assumed to be 10 μm (a commonly assumed value for cavitation calculations [45]) and fluid conditions similar to those inside the membrane module were applied.
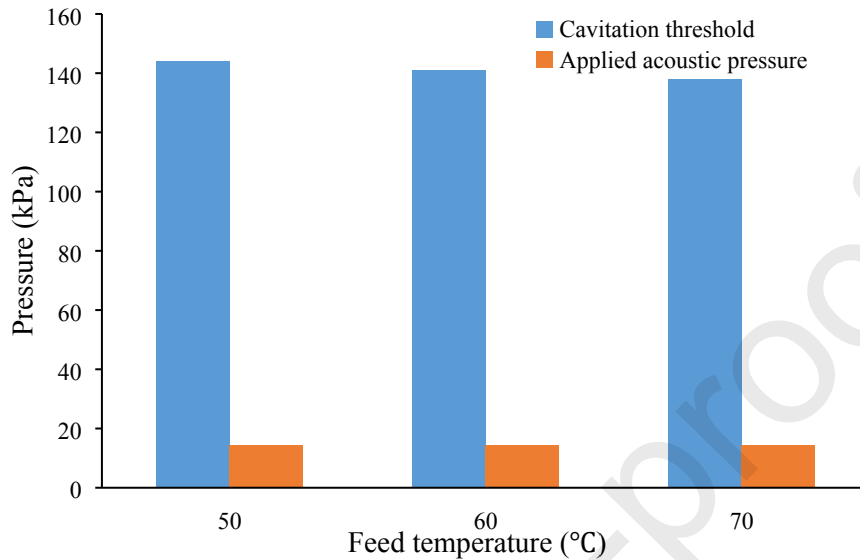

Fig. 8. Comparison between cavitation threshold and generated acoustic pressure for the highest applied ultrasonic power (23W), for feed water at 50°C, 60°C and 70°C.

As seen in Fig. 8, there is a significant difference between the cavitation threshold and the generated acoustic pressure at the highest applied level. Hence, the permeate flux improvement is likely to be attributed to the cleaning effects and the mass transfer enhancements caused by acoustic streaming. Previous studies applied high power level and proposed that ultrasound benefits were due to some or all of cavitational effects such as micro streaming, and thermal effects [28, 70]. A comparison has been drawn between the flux enhancement obtained in this study with those reported in the literature, taking into consideration the experimental conditions and the specifications of the membrane and ultrasound setup as shown in Table 3. It can be seen that the performance of the proposed direct ultrasonic-assisted AGMD configuration in this study exceeded by far the performance of other reported configurations. With directly applied ultrasound, a low power level of 8 W resulted in higher flux improvement than the indirect ultrasound approaches, where the power applied was as high as 260 W. The reason behind this is that direct ultrasound has minimal transfer power loss compared to other configurations, where a significant part of the power is lost in irradiating the transmitting media (water or module body). These losses make

23

ultrasound technology seems to be an energy intensive practice and a challenge to scale to an industrial level.

Table 3: Flux enhancement and experimental conditions of current study vs previous studies

Experimental conditions						Membrane configuration	Maximum flux enhancement	US setup	Study
Power (W)	Frequency (kHz)	Feed temperature (℃)	Coolant temperature (℃)	Feed flowrate	Sample type				
8	17.8	70	20	0.092 m/s	Natural groundwater	AGMD	100%	Direct irradiation	Current study
260	20	53	20	0.250 m/s	150 mg/L Na$_2$SiO$_3$	DCMD	20%	Indirect through water bath	[36]
260	20	53	20	0.250 m/s	140 g/L NaCl	DCMD	60%	Indirect through water bath	[35]
100	20	40	25	0.063 m/s	5 wt% NaCl	AGMD	200%	Indirect through the module body	[37]

Several factors can influence the efficiency of ultrasound treatment, namely orientation and position of the ultrasonic field, ultrasonic power intensity and frequency, type of membrane and fouling materials, membrane housing, and operating pressure [7]. The focus of our study is on varying ultrasonic power within a low, energy efficient and membrane damage-free range. Ultrasound was applied to vibrate the slotted stainless-steel spacer plate of 1 mm thickness, which was placed between the membrane surface and coolant side. At a time when ultrasound was applied, the spacers started shaking immediately on both sides of membrane as a result of ultrasonic waves passage. The foulants which tend to deposit on the membrane surface during the normal AGMD operation were detached/dislodged due to vibration in the ultrasonic assisted AGMD, and then carried away with the feedwater flow. This resulted in a clean membrane surface and an improved vapor flux. It should be noted here that with the proposed direct ultrasonic-assisted AGMD process there is no risk of permeate contamination due to the passage of detached scale particles and this is evident in the consistent high rejection percentage of cleaned membranes presented in Figs 4-7 (data presented in square marks). When considering the forces acting on detached scale particles in tangential flow filtration, as in this study, there is only a weak drag force resulting from water vapour flow from feed side to the permeate side [71] in comparison to two strong forces that push the particle to the feed side; the force resulting from the tangential flow of the feed and the force generated from acoustic streaming. Hence, even particles with smaller size than the membrane pores are unlikely to pass through the membrane. The nature of the polymeric membrane being such that it only permits the passage of water vapour, provides another protection layer preventing the flow of detached salt into the permeate side, as they exist as dissolved i.e. not in vapour format. Regarding the concentrated stream of rejected salt, it is typically discharged into the environment with different ways of disposal, such as marine, well injection and solar evaporation ponds. When strict environmental regulations are applied, the concentrated stream may be further treated with zero liquid discharge processes such as crystallization.

An additional advantage for the use of ultrasound in AGMD is that the energy of the ultrasound is transformed to heat which can improve heat transfer from the hot side to the coolant side [72], contributing to the direct membrane surface heating. Once the heat transfer loss is reduced as a result of ultrasound energy, the feed water temperature will be maintained constant which will further reduce temperature drop/loss inside the module thereby reducing temperature polarization effect [73]. This condition would further lead to increasing the mass transfer through the membrane.

26

The effects of applying various ultrasound powers ranging from 8 to 23 W, on RW permeate flux for PTFE membranes were investigated and the results are presented in Fig. 9. PTFE was selected in this step of the investigation due to it is durable structure for ultrasound application [35]. Fig. 9 shows that the permeate flux almost doubled from 0.65 kg/m^2.h to 1.19 kg/m^2.h by increasing the power from 8 to 23 W. Flux increments exhibited a logarithmic behaviour with ultrasound increase and this agrees with the reported findings in [37]. The increment of ultrasound power did not damage the membrane surface as verified by the membrane surface visualisation tests (see Fig. 12). Kobayashi et al. [74] observed a significant increase in ultrafiltration flux using a power intensity of 23 W/cm^2 with no membrane damage. Ultrasound should be used carefully because polymeric materials could get effect by applying high frequency and power.
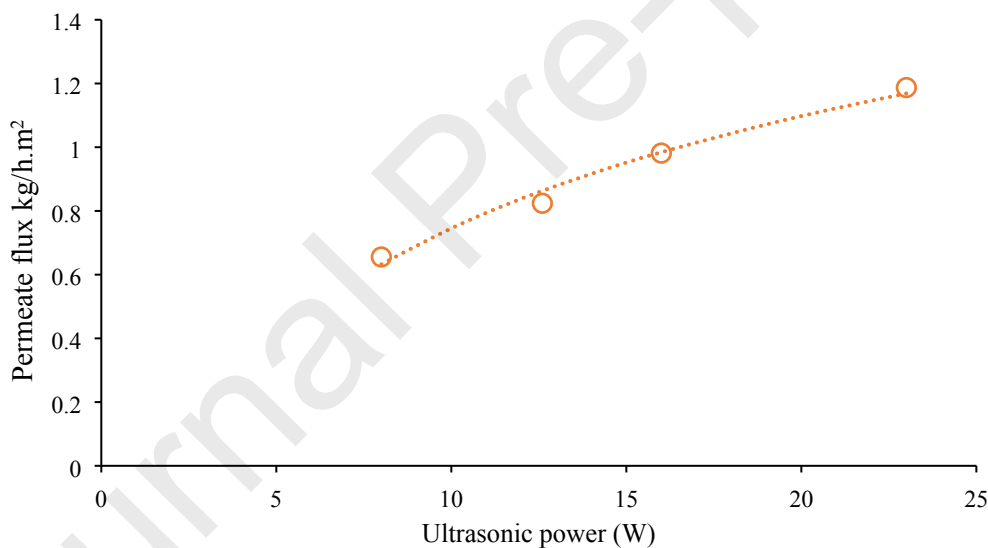

Fig.9. Effect of applied ultrasound power on permeate flux for RW, Feedwater = 60°C at 100 L/h, Coolant = 20°C at 200 L/h.

The effect of ultrasound on mass transfer was estimated theoretically by computing the overall mass transfer coefficient of AGMD with and without ultrasound using equation 3-13. The ratio of the coefficients of the two treatment scenarios (enhancement ratio) was calculated and plotted against the applied power level as illustrated in Fig. 10. It can be seen from this figure that the trend of the enhancement ratio is similar to that of flux increment in Fig.9 confirming that the flux improvement is attributed to ultrasound effect on mass transfer.
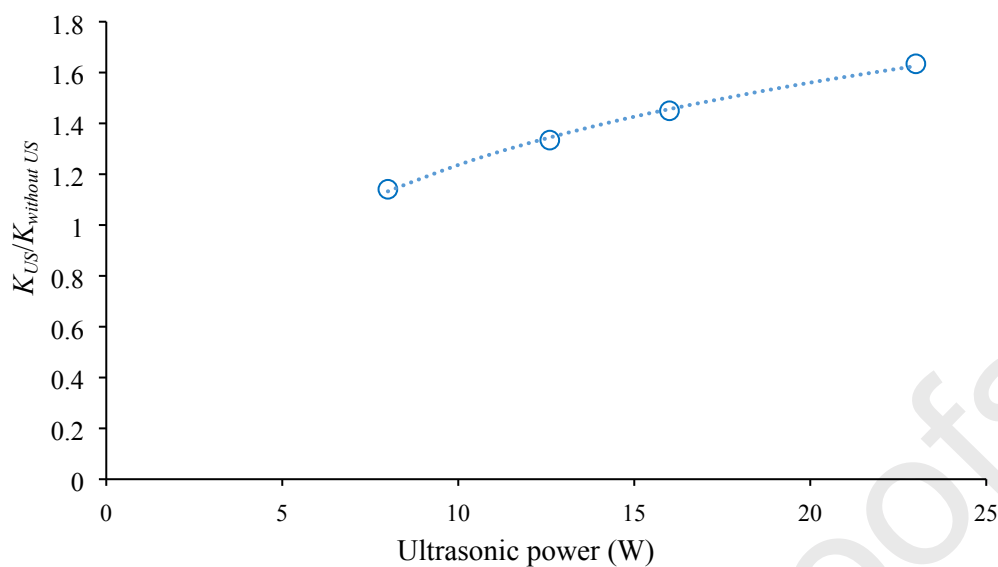
Fig. 10. Enhancement ratio with varying ultrasonic power levels

4.5. *ATR FT-IR analysis of membrane surface*

ATR FT-IR was employed in this study to evaluate the change in surface chemistry of PTFE membranes before and after ultrasound treatments. ATR FT-IR spectra of virgin, fouled and cleaned PTFE membrane surfaces are shown in Fig.11. The spectra of virgin membranes revealed the presence of a set of peaks which are characteristic of the PTFE material used (Fig. 11 a). The bands at 1199 and 1146 cm^{-1} were assigned to CF$_2$, symmetric stretching vibrations [75], while the band at 640 cm^{-1} was attributed to the rolling vibrations of the CF$_2$ group [76]. The band at 553 cm^{-1} corresponded to CF$_2$ deformation [76]. The wide band appearing in the spectrum of the fouled membrane at 1001 cm^{-1} (Fig. 11 b) could be attributed to silica precipitation [77] and/or gypsum scaling (CaSO$_4$·2H$_2$O) [78]. Both contaminants are present in the feed water (Table 1) and they are known for their tendency to foul MD membranes [79, 80]. Silica fouling potency increases when the concentration exceeds the amorphous silica concentration range of 100-140 mg/L [81] and this is the case in this study (see Table 1). Comparing spectra of the fouled and ultrasonically cleaned membranes (Figs. 11b and c), it can be clearly seen that ultrasound was very effective in removing foulants from the membrane surface. The characteristic PTFE peaks which were supressed in the spectrum of the fouled membrane (Fig. 11b), fully reappeared in the spectrum of the cleaned membrane (Fig. 11c). Ultrasound exhibited superior performance in removing silica/gypsum fouling. As seen in Fig. 11c, the intensity of the band at 1001 cm^{-1} was significantly reduced after ultrasound treatment compared to that of the fouled membrane

28

(Fig. 11 b). This is an important finding as it points out that ultrasonic-assisted membrane cleaning could be a feasible tool in eliminating persistent membrane foulants which are difficult to remove by other existing cleaning techniques.
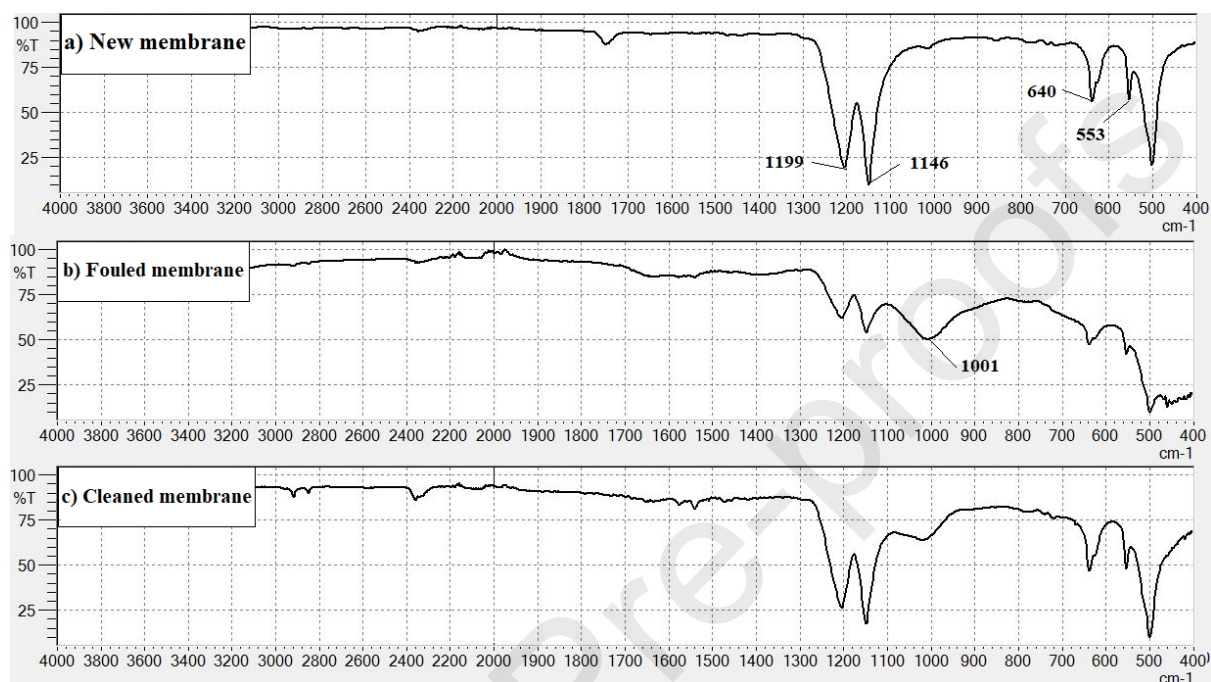

Fig. 11. ATR FTIR spectra of (a) virgin PTFE membrane, (b) fouled PTFE membrane, and (c) ultrasonically cleaned PTFE membrane.

4.6. Membrane surface characterization

A scanning electron microscope technique was employed in this study to examine the morphological changes of the membrane surface, before and after ultrasound treatments. Fig. 12 shows the surfaces of virgin, fouled and ultrasound-treated PTFE membranes. Significant fouling was observed on the surface of membranes after 70 h of operation (Fig. 12 b) compared to the clean surface of the virgin membrane (Fig. 12 a). The subsequent ultrasound treatment effectively removed the fouling layer from the membrane surface as seen in Fig. 12 c. Also, no signs of damage to the membrane surface were observed, confirming that applying direct, low power ultrasound did not affect membrane integrity, unlike other studies that reported damage to membrane construction materials due to the high level of applied ultrasonic power [30, 65].
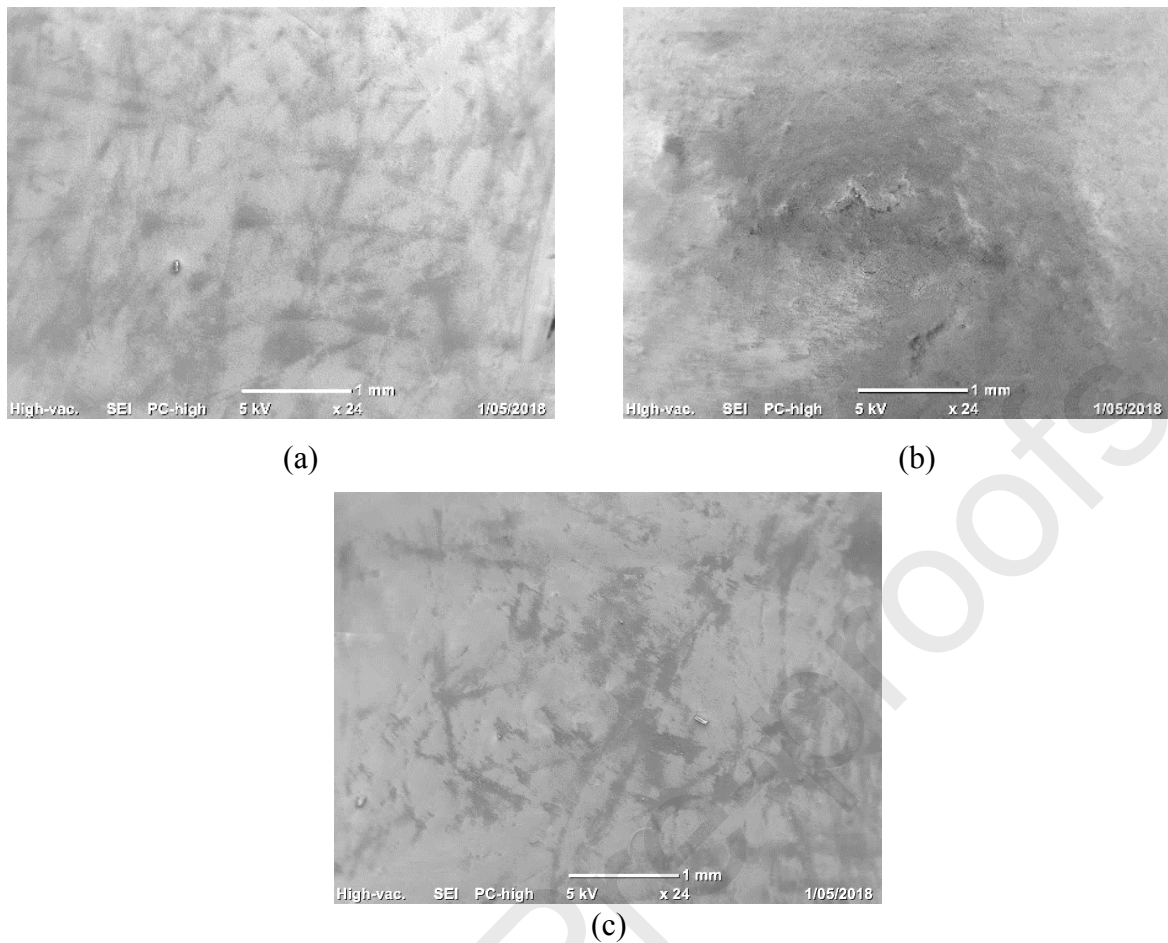
(a)

(b)

(c)

Fig. 12. SEM images of (a) virgin, (b) fouled, and (c) ultrasonically cleaned PTFE membranes.

5. Conclusions

The effect of ultrasound with an applied power range of 8 - 23 W, on membrane fouling and permeate flux enhancements for an AGMD system were investigated for three different levels of feedwater flowrate and temperature. NW and RW were treated using PTFE and PVDF membrane types. Generally, NW had higher flux compared to RW. As expected from published literature, the higher the feedwater temperature and flowrate, the higher the permeate flux produced. Ultrasound application improved permeate flux of all treatment scenarios, due to cleaning effects and mass transfer enhancements. ATR FT-IR analyses showed that the ultrasound treatment effectively removed foulants from the membrane surface. SEM visualisation revealed that ultrasound treatments did not exert any negative effects on treated membranes' integrity and was able to return a significantly fouled membrane back to close to pristine status. This study also showed that the ultrasonic-assisted

30

AGMD process was effective in treating water samples with very different physicochemical properties. Continuing research into finding effective ways of applying ultrasound for fouling mitigation and flux enhancement in AGMD and other membrane systems is recommended for future endeavours. As always, such applications should be practical in their implementation, relevant at an industrial scale and utilise ultrasonic energy wisely. Some aspects that are recommended for exploration are theoretical modelling of the ultrasonic-assisted AGMD process and the effect of frequency and different module configurations on process   performance.

References

[1] L. Camacho, L. Dumée, J. Zhang, J.-d. Li, M. Duke, J. Gomez, S. Gray, Advances in membrane distillation for water desalination and purification applications, Water, 5 (2013) 94-196.

[2] A.S. Alsaadi, L. Francis, H. Maab, G.L. Amy, N. Ghaffour, Evaluation of air gap membrane distillation process running under sub-atmospheric conditions: Experimental and simulation studies, Journal of Membrane Science, 489 (2015) 73-80.

[3] H. Susanto, Towards practical implementations of membrane distillation, Chemical Engineering and Processing: Process Intensification, 50 (2011) 139-150.

[4] J.B. Gálvez, L. García-Rodríguez, I. Martín-Mateos, Seawater desalination by an innovative solar-powered membrane distillation system: the MEDESOL project, Desalination, 246 (2009) 567-576.

[5] J. Xu, N.S. Bettahalli, S. Chisca, M.K. Khalid, N. Ghaffour, R. Vilagines, S.P. Nunes, Polyoxadiazole hollow fibers for produced water treatment by direct contact membrane distillation, Desalination, 432 (2018) 32-39.

[6] R.A. Johnson, M.H. Nguyen, Understanding Membrane Distillation and Osmotic Distillation, John Wiley & Sons, 2017.

[7] M.O. Lamminen, H.W. Walker, L.K. Weavers, Mechanisms and factors influencing the ultrasonic cleaning of particle-fouled ceramic membranes, Journal of membrane science, 237 (2004) 213-223.

[8] H.-C. Flemming, G. Schaule, R. McDonogh, H.F. Ridgway, Effects and extent of biofilm accumulation in membrane systems, Biofouling and biocorrosion in industrial water systems, (1994) 63-89.

[9] J.-G. Lee, A.S. Alsaadi, A.M. Karam, L. Francis, S. Soukane, N. Ghaffour, Total water production capacity inversion phenomenon in multi-stage direct contact membrane distillation: A theoretical study, Journal of Membrane Science, 544 (2017) 126-134.

[10] D.M. Warsinger, J. Swaminathan, E. Guillen-Burrieza, H.A. Arafat, Scaling and fouling in membrane distillation for desalination applications: a review, Desalination, 356 (2015) 294-313.

[11] R.D. Noble, S.A. Stern, Membrane separations technology: principles and applications, Elsevier, 1995.

[12] W. Ho, K. Sirkar, Membrane Handbook Van Nostrand Reinhold New York Google Scholar, (1992).

[13] Z. Zhu, W. Wang, D. Qi, Y. Luo, Y. Liu, Y. Xu, F. Cui, C. Wang, X. Chen, Calcinable Polymer Membrane with Revivability for Efficient Oily-Water Remediation, Advanced Materials, (2018) 1801870.

[14] M. Gryta, Alkaline scaling in the membrane distillation process, Desalination, 228 (2008) 128-134.

[15] L. Fortunato, Y. Jang, J.-G. Lee, S. Jeong, S. Lee, T. Leiknes, N. Ghaffour, Fouling development in direct contact membrane distillation: Non-invasive monitoring and destructive analysis, Water research, (2017).

[16] J. Li, R. Sanderson, E. Jacobs, Ultrasonic cleaning of nylon microfiltration membranes fouled by Kraft paper mill effluent, Journal of Membrane Science, 205 (2002) 247-257.

[17] A.M. Alklaibi, N. Lior, Membrane-distillation desalination: status and potential, Desalination, 171 (2005) 111-131.

[18] A. Razmjou, E. Arifin, G. Dong, J. Mansouri, V. Chen, Superhydrophobic modification of TiO2 nanocomposite PVDF membranes for applications in membrane distillation, Journal of membrane science, 415 (2012) 850-863.

[19] G. Amy, N. Ghaffour, Z. Li, L. Francis, R.V. Linares, T. Missimer, S. Lattemann, Membrane-based seawater desalination: Present and future prospects, Desalination, 401 (2017) 16-21.

[20] T. Kuehn, D. Kittelson, Y. Wu, R. Gouk, Particle removal from semiconductor wafers by megasonic cleaning, Journal of Aerosol Science, 27 (1996) S427-S428.

[21] E. Tarleton, R.J. Wakeman, Microfiltration enhancement by electrical and ultrasonic force fields, Filtration & Separation, 27 (1990) 192-194.

[22] X. Chai, T. Kobayashi, N. Fujii, Ultrasound-associated cleaning of polymeric membranes for water treatment, Separation and Purification Technology, 15 (1999) 139-146.

[23] D. Chen, Z. He, L.K. Weavers, Y.-P. Chin, H.W. Walker, P.G. Hatcher, Sonochemical reactions of dissolved organic matter, Research on chemical intermediates, 30 (2004) 735-753.

[24] I. Tsukamoto, B. Yim, C. Stavarache, M. Furuta, K. Hashiba, Y. Maeda, Inactivation of Saccharomyces cerevisiae by ultrasonic irradiation, Ultrasonics sonochemistry, 11 (2004) 61-65.

[25] P.R. Gogate, A.M. Kabadi, A review of applications of cavitation in biochemical engineering/biotechnology, Biochemical Engineering Journal, 44 (2009) 60-72.

[26] T. Yusaf, R.A. Al-Juboori, Alternative methods of microorganism disruption for agricultural applications, Applied Energy, 114 (2014) 909-923.

[27] V. Naddeo, A. Cesaro, D. Mantzavinos, D. Fatta-Kassinos, V. Belgiorno, Water and wastewater disinfection by ultrasound irradiation-a critical review, Global NEST Journal, 16 (2014) 561-577.

[28] M. Qasim, N. Darwish, S. Mhiyo, N. Darwish, N. Hilal, The use of ultrasound to mitigate membrane fouling in desalination and water treatment, Desalination, 443 (2018) 143-164.

[29] S.K. Sharma, D. Chen, A. Mudhoo, Handbook on applications of ultrasound: sonochemistry for sustainability, CRC press, 2011.

[30] D. Chen, L.K. Weavers, H.W. Walker, Ultrasonic control of ceramic membrane fouling by particles: effect of ultrasonic factors, Ultrasonics sonochemistry, 13 (2006) 379-387.

[31] M. Mohsin, M. Meribout, An extended model for ultrasonic-based enhanced oil recovery with experimental validation, Ultrasonics Sonochemistry, 23 (2015) 413-423.

[32] M. Mohsin, M. Meribout, Oil–water de-emulsification using ultrasonic technology, Ultrasonics Sonochemistry, 22 (2015) 573-579.

[33] M. Meribout, On Using Ultrasonic-assisted Enhanced Oil Recovery (EOR): Recent Practical Achievements and Future Prospects, IEEE Access, 6 (2018) 51110-51118.

[34] M. Legay, N. Gondrexon, S. Le Person, P. Boldo, A. Bontemps, Enhancement of heat transfer by ultrasound: review and recent advances, International Journal of Chemical Engineering, 2011 (2011).

[35] D. Hou, G. Dai, H. Fan, H. Huang, J. Wang, An ultrasonic assisted direct contact membrane distillation hybrid process for desalination, Journal of Membrane Science, 476 (2015) 59-67.

[36] D. Hou, Z. Wang, G. Li, H. Fan, J. Wang, H. Huang, Ultrasonic assisted direct contact membrane distillation hybrid process for membrane scaling mitigation, Desalination, 375 (2015) 33-39.

[37] C. Zhu, G. Liu, Modeling of ultrasonic enhancement on membrane distillation, Journal of Membrane Science, 176 (2000) 31-41.

[38] R.A. Al-Juboori, L.A. Bowtell, T. Yusaf, V. Aravinthan, Insights into the scalability of magnetostrictive ultrasound technology for water treatment applications, Ultrasonics sonochemistry, 28 (2016) 357-366.

[39] S. Adnan, M. Hoang, H. Wang, Z. Xie, Commercial PTFE membranes for membrane distillation application: Effect of microstructure and support material, Desalination, 284 (2012) 297-308.

[40] L.M. Camacho, L. Dumée, J. Zhang, J.-d. Li, M. Duke, J. Gomez, S. Gray, Advances in Membrane Distillation for Water Desalination and Purification Applications, 5 (2013) 94-196.

[41] R.A. Al-Jubooria, T. Yusafb, L.J.D. Bowtellc, W. TREATMENT, Pulsed ultrasound as an energy saving mode for ultrasound treatment of surface water with terrestrial aquatic carbon, 135 (2018) 167-176.

[42] R.A. Al-Juboori, L. Bowtell, Ultrasound Technology Integration into Drinking Water Treatment Train, in: Sonochemical Reactions, IntechOpen, 2019.

[43] R.A. Al-Juboori, T. Yusaf, L. Bowtell, Energy Conversion Efficiency of Pulsed Ultrasound, Energy Procedia, 75 (2015) 1560-1568.

[44] I. Masselin, X. Chasseray, L. Durand-Bourlier, J.-M. Lainé, P.-Y. Syzaret, D. Lemordant, Effect of sonication on polymeric membranes, Journal of membrane science, 181 (2001) 213-220.

[45] A. Al-Juboori Raed, T. Yusaf, Identifying the Optimum Process Parameters for Ultrasonic Cellular Disruption of E. Coli, in: International Journal of Chemical Reactor Engineering, 2012.

[46] R.A. Al-Juboori, T. Yusaf, Identifying the optimum process parameters for ultrasonic cellular disruption of E. coli, International Journal of Chemical Reactor Engineering, 10 (2012).

[47] J. Phattaranawik, R. Jiraratananon, A.G. Fane, Heat transport and membrane distillation coefficients in direct contact membrane distillation, Journal of Membrane Science, 212 (2003) 177-193.

[48] J. Krautkrämer, H. Krautkrämer, Ultrasonic testing of materials, Springer Science & Business Media, 2013.

[49] M. Khayet, T. Matsuura, Membrane distillation: principles and applications, Elsevier, 2011.

[50] S.O. Olatunji, L.M. Camacho, Heat and Mass Transport in Modeling Membrane Distillation Configurations: A Review, 6 (2018).

[51] E. Curcio, E. Drioli, Membrane Distillation and Related Operations—A Review, Separation & Purification Reviews, 34 (2005) 35-86.

[52] C.B. Baxi, A.J.J.o.H.T. Ramachandran, Effect of vibration on heat transfer from spheres, 91 (1969) 337-343.

[53] A. Sathyabhama, S.J.H.T.A.R. Prashanth, Enhancement of boiling heat transfer using surface vibration, 46 (2017) 49-60.

[54] R. Schofield, A. Fane, C.J.J.o.M.S. Fell, Gas and vapour transport through microporous membranes. I. Knudsen-Poiseuille transition, 53 (1990) 159-171.

[55] H. Attia, M.S. Osman, D.J. Johnson, C. Wright, N.J.D. Hilal, Modelling of air gap membrane distillation and its application in heavy metals removal, 424 (2017) 27-36.

[56] R.W. Schofield, A.G. Fane, C.J.D. Fell, Heat and mass transfer in membrane distillation, Journal of Membrane Science, 33 (1987) 299-313.

[57] R. Thanedgunbaworn, R. Jiraratananon, M.H.J.I.J.o.F.E. Nguyen, Vapour transport mechanism in osmotic distillation process, 5 (2009).

[58] F.A. Banat, J. Simandl, Desalination by Membrane Distillation: A Parametric Study, Separation Science and Technology, 33 (1998) 201-226.

[59] C. Zhu, G.L. Liu, C.S. Cheung, C.W. Leung, Z.C. Zhu, Ultrasonic stimulation on enhancement of air gap membrane distillation, Journal of Membrane Science, 161 (1999) 85-93.

[60] A.M. Alklaibi, N. Lior, Transport analysis of air-gap membrane distillation, Journal of membrane science, 255 (2005) 239-253.

[61] J. Xu, Y.B. Singh, G.L. Amy, N. Ghaffour, Effect of operating parameters and membrane characteristics on air gap membrane distillation performance for the treatment of highly saline water, Journal of Membrane Science, 512 (2016) 73-82.

[62] L. Martínez-Díez, M.I.J.J.o.m.s. Vazquez-Gonzalez, Temperature and concentration polarization in membrane distillation of aqueous salt solutions, 156 (1999) 265-273.

[63] Y. Tao, D.-W. Sun, Enhancement of food processes by ultrasound: a review, Critical Reviews in Food Science and Nutrition, 55 (2015) 570-594.

[64] S. Muthukumaran, K. Yang, A. Seuren, S. Kentish, M. Ashokkumar, G.W. Stevens, F. Grieser, The use of ultrasonic cleaning for ultrafiltration membranes in the dairy industry, Separation and Purification Technology, 39 (2004) 99-107.

[65] H. Kyllönen, P. Pirkonen, M. Nyström, Membrane filtration enhanced by ultrasound: a review, Desalination, 181 (2005) 319-335.

[66] E. Tarleton, R.J. Wakeman, Y. Liang, Electrically enhanced washing of ionic species from fine particle filter cakes, Chemical Engineering Research and Design, 81 (2003) 201-210.

[67] A.S. Alsaadi, N. Ghaffour, J.-D. Li, S. Gray, L. Francis, H. Maab, G.L. Amy, Modeling of air-gap membrane distillation process: A theoretical and experimental study, Journal of membrane science, 445 (2013) 53-65.

[68] S. Yarlagadda, L.M. Camacho, V.G. Gude, Z. Wei, S. Deng, Membrane distillation for desalination and other separations, Recent Patents on Chemical Engineering, 2 (2009) 128-158.

[69] B. Sajjadi, S. Asgharzadehahmadi, P. Asaithambi, A.A.A. Raman, R. Parthasarathy, Investigation of mass transfer intensification under power ultrasound irradiation using 3D computational simulation: A comparative analysis, Ultrasonics sonochemistry, 34 (2017) 504-518.

[70] M.O. Lamminen, H.W. Walker, L.K. Weavers, Cleaning of particle-fouled membranes during cross-flow filtration using an embedded ultrasonic transducer system, Journal of Membrane Science, 283 (2006) 225-232.

[71] J.S. Knutsen, R.H. Davis, Deposition of foulant particles during tangential flow filtration, Journal of Membrane Science, 271 (2006) 101-113.

[72] J. Berlan, T.J. Mason, Sonochemistry: from research laboratories to industrial plants, Ultrasonics, 30 (1992) 203-212.

[73] A.S. Alsaadi, L. Francis, G.L. Amy, N. Ghaffour, Experimental and theoretical analyses of temperature polarization effect in vacuum membrane distillation, Journal of Membrane Science, 471 (2014) 138-148.

[74] T. Kobayashi, T. Kobayashi, Y. Hosaka, N. Fujii, Ultrasound-enhanced membrane-cleaning processes applied water treatments: influence of sonic frequency on filtration treatments, Ultrasonics, 41 (2003) 185-190.

[75] A. Alpatova, M. Meshref, K.N. McPhedran, M. Gamal El-Din, Composite polyvinylidene fluoride (PVDF) membrane impregnated with Fe2O3 nanoparticles

and multiwalled carbon nanotubes for catalytic degradation of organic contaminants, Journal of Membrane Science, 490 (2015) 227-235.

[76] D.D. Fazullin, G.V. Mavrin, M.P. Sokolov, I.G. Shaikhiev, Infrared spectroscopic studies of the PTFE and nylon membranes modified polyaniline Modern Applied Science, 9 (2015) 242-249.

[77] F.A. Miller, C.H. Wilkins, Infrared Spectra and Characteristic Frequencies of Inorganic Ions, Analytical Chemistry, 24 (1952) 1253-1294.

[78] J. Coates, Interpretation of Infrared Spectra, A Practical Approach, John Wiley & Sons, Ltd, U.S.A., 2006.

[79] J. Gilron, Y. Ladizansky, E. Korin, Silica Fouling in Direct Contact Membrane Distillation, Industrial & Engineering Chemistry Research, 52 (2013) 10521-10529.

[80] E. Curcio, X. Ji, G. Di Profio, A.O. Sulaiman, E. Fontananova, E. Drioli, Membrane distillation operated at high seawater concentration factors: Role of the membrane on $CaCO_3$ scaling in presence of humic acid, Journal of Membrane Science, 346 (2010) 263-269.

[81] D. Hou, L. Zhang, C. zhao, H. Fan, J. Wang, H. Huang, Ultrasonic irradiation control of silica fouling during membrane distillation process, Desalination, 386 (2016) 48-57.

Highlights:

- Air-gap membrane distillation was used to treat RO reject and natural ground water.
- Various feed temperature and flow rate were tested with two commercial membranes.
- Low ultrasounic power was directly applied through spacers.
- Ultrasound improved the flux by 100% for fouled membranes.
- Fouling was decreased without membrane damage.